

## Chapter 3

# LHC AND THE ATLAS DETECTOR

Among the principal instruments of modern experimental particle physics are accelerators and detectors. In accelerators, particles are accelerated to some energy before being made to collide, and the collision debris in the form of new particles are collected and analysed in the detectors. A high centre-of-mass energy, which is required in order that high mass scale physics may be reached, leads to many technical challenges that need to be overcome as well as the overall complexity of modern accelerators and detectors.

This chapter discusses the Large Hadron Collider (LHC) based at CERN and the ATLAS detector, one among the four main detectors located at the LHC.

### 3.1 CERN AND THE LARGE HADRON COLLIDER

Broadly speaking, the development of physics rests upon two sources, the first, the availability of a set of physical phenomena and the second, active theoretical investigations. At the turn of the 20th century, atomic phenomena confirmed the discrete nature of physical quantities previously thought to be continuous and motivated the development of quantum mechanics. Subsequently, the quest to unify quantum mechanics and special relativity, in parallel with probes into sub-atomic phenomena, led to the development of quantum field theory and eventually gave birth to the Standard Model of particle physics. At present, more than ever before, both technological advances and active theoretical investigations are being pushed to the limit to scrutinize the Standard Model and go beyond it. In this respect, the Large Hadron Collider based at CERN has been playing a leading role, being the most powerful collider at the moment.

CERN [27], also known as European Organization for Nuclear Research, was established in the post-war era, the 1940s, to foster physics development and scientific collaboration in Europe. The Large Hadron Collider [28], built in the period 1984-1989 at CERN, was designed to explore physics beyond the Standard Model. It is a complex of successive accelerators that increase the accelerated particle energy by approximately an order of magnitude at each pass from one accelerator to the next.

The LHC reuses the Large Electron Position (LEP) tunnel, which produced  $e^+e^-$  collisions, and is 26.7 km in circumference and lies between 45 m and 170 m underground. The designed centre of mass energy is 14 TeV, at which Higgs physics and some beyond the Standard Model physics become accessible. It has two rings with counter-rotating proton beams. The beams are accelerated by a high-frequency standing wave, and by design take the form of bunches of particles, which are spaced by 25 ns and each of which contains up to  $1.1 \times 10^{11}$  protons. The beam particles are kept along a circular trajectory and are focused near the collision points using dipole and quadrupole magnets. Notable at the LHC is the use of superconducting magnets that operate at 2K and lower.

Figure 3.1 shows the CERN's accelerator complex. The four main detectors are ATLAS, CMS, ALICE, and LHCb, all located at different collision points. Among them, the high luminosity experiments are ATLAS and CMS.

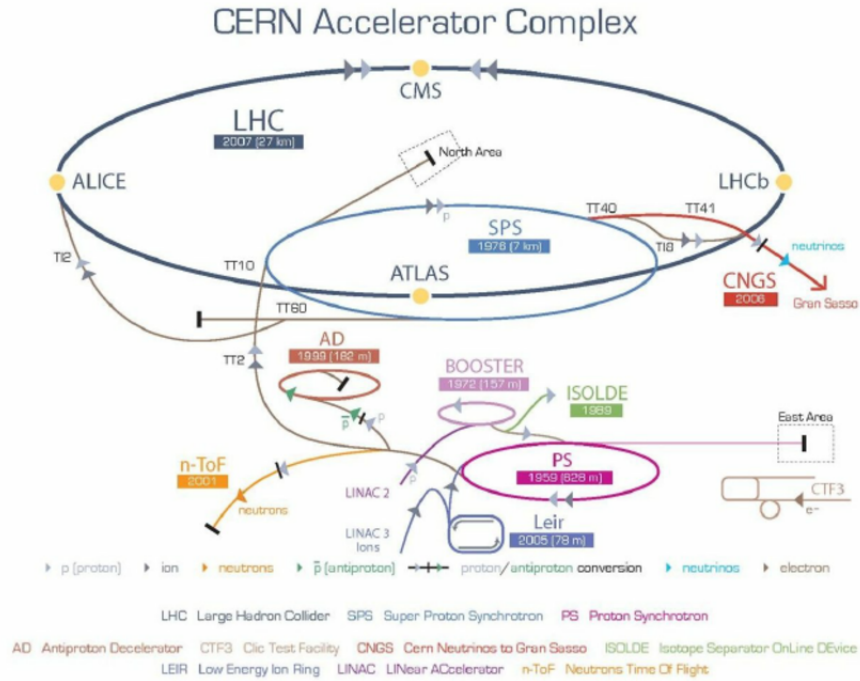


Figure 3.1: CERN's Accelerator Complex  
[31]

Initially in Run-1 (2010-2012), the LHC was operating at 7 and 8 TeV center-of-mass energy. The superconducting beampipe magnets were upgraded during the long shutdown 2012-2015, helping to reach 13 TeV center-of-mass energy in Run-2 (2015-2018). Following Run-2 is another shutdown (2019-2020), during which upgrades are performed in preparation for Run-3 (2021-2023).

At the end Run-2 a total of approximately  $160\text{fb}^{-1}$  of data was delivered by the LHC. This total luminosity, denoted  $L$ , is proportional to the number of events  $N$  produced for a physics process with cross section  $\sigma$ , according to the formula

$$N = \sigma L$$

588 The number of events produced per unit time is a function of the instantaneous  
 589 luminosity  $L_I$  which is related to  $L$  by

$$L = \int L_I dt$$

590 The LHC was designed to achieve high luminosity. In general, given two colliding  
 591 beams with  $N_1$  and  $N_2$  number of particles, a general formula for the instantaneous  
 592 luminosity, assuming Gaussian profiles of the beams, is

$$L_I = f \frac{N_1 N_2}{4\pi\sigma_x\sigma_y}$$

593 where

- 594 •  $f$  is the frequency at which the beams collide
- 595 •  $\sigma_x$  and  $\sigma_y$  are the root-mean-square horizontal and vertical beam sizes.

596 On the other hand, we need to deal with so-called pileup events that come from  
 597 high luminosity. They are undesired events on top of the hard scattering, and may  
 598 occur in two scenarios. Either many interactions occur in each collision, in which  
 599 case we have in-time pileup, or interactions that belong to different collisions are  
 600 (incorrectly) recorded together, in which case we have out-of-time pileup.

## 601 3.2 THE ATLAS DETECTOR

602 ATLAS [29] is a general-purpose detector located at one among several collision  
 603 points at the LHC. The LHC, at 14 TeV designed centre-of-mass energy, is capable of  
 604 probing not only Higgs physics but also some beyond Standard Model physics. Since  
 605 the new hypothetical particles are typically expected to decay to energetic Standard  
 606 Model particles, ATLAS is designed to be able to identify and measure important  
 607 physics objects such as photons, electrons, muons, taus, hadronic jets, and neutrinos  
 608 and other weakly interacting particles in the form of missing transverse energy. In  
 609 addition, with regard to jets, it needs to be able to distinguish between heavy flavour  
 610 jets ( $b$  and  $c$  quarks) and other light jets.

611 An overview of the ATLAS detector is shown in Figure 3.2. It is 25 m in diameter  
 612 and 44 m in length, and weights approximately 7000 tons.

613 In conformity with modern detector design, ATLAS is made up of a number of  
 614 subsystems that surround one another in layers. Innermost is the inner detector,  
 615 or the tracker. Next, in order, are the electromagnetic calorimeter, the hadronic  
 616 calorimeter, and the muon chamber. These subsystems work in combination to  
 617 provide detection capability in many possible physics scenarios. They are built out  
 618 of components that are fast, precise, and that can stand against high radiation.  
 619 Moreover, they are supplemented by an efficient trigger system.

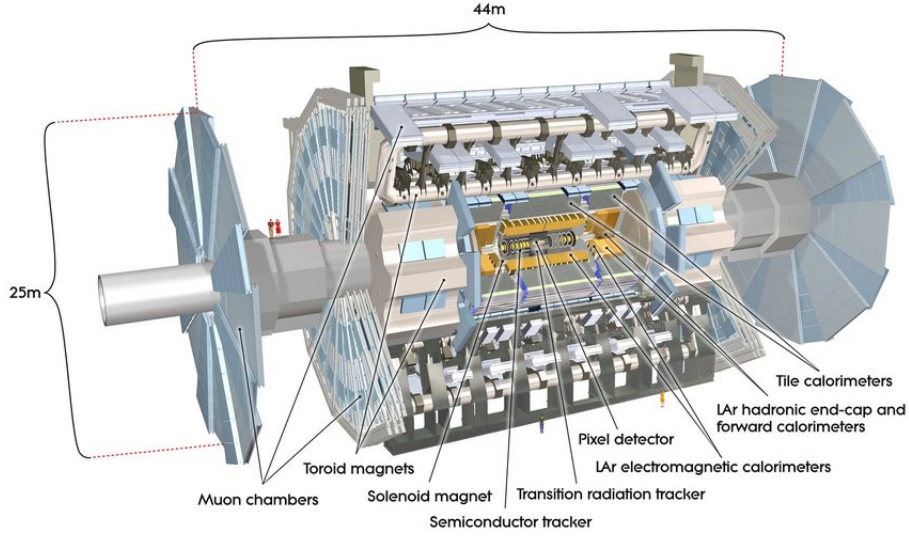


Figure 3.2: The ATLAS Detector  
[32]

The entire detector is nominally forward-backward symmetric with respect to the interaction point. The magnet configuration, which determines the overall design of the detector, consists of

- A thin superconducting solenoid that surrounds the inner-detector cavity,
- Three large superconducting toroids around the calorimeters, arranged with an eight-fold azimuthal symmetry.

### 3.2.1 The ATLAS Coordinate System

Each nominal interaction is given a coordinate system [29], where

- The origin is taken to be the interaction point;
- The  $z$ -axis is defined by the beam direction

Thus the  $x - y$  plane is transverse to the beam direction. The positive  $x$ -axis points from the interaction point to the centre of the LHC ring. The positive  $y$ -axis points upwards.

The following quantities are used to reconstruct the kinematic Lorentz vectors of the final state particles; some of them are illustrated in Figure 3.3, which also illustrates the ATLAS coordinate system.

- The azimuthal angle  $\phi$ ,
- The polar angle  $\theta$ ,

- The rapidity

$$y = \frac{1}{2} \ln \left( \frac{E + p_z}{E - p_z} \right),$$

whose difference is invariant with respect to boosts along the  $z$ -direction. In high-energy collisions the produced particles are expected to be more and more perpendicular to the beam-axis, and their rapidities will then be closer and closer to zero.

- The pseudorapidity

$$\eta = -\ln \left( \tan \frac{\theta}{2} \right),$$

For a highly-energetic particle  $\eta$  almost coincides with  $y$  but is much easier to measure.

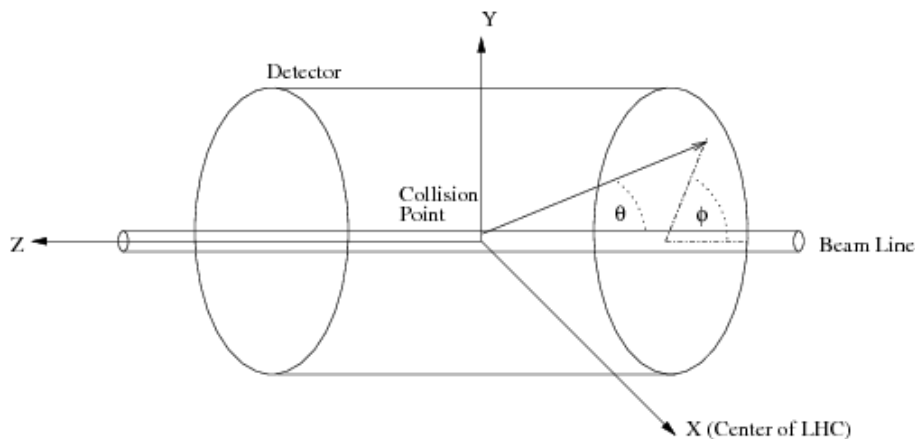


Figure 3.3: The ATLAS Coordinate System []

In the transverse plane perpendicular to the beam-axis the transverse momenta and the transverse energy are defined according to the formulas

$$p_T = p \sin \theta, \quad E_T = E \sin \theta$$

Distances in the  $\eta - \phi$ -plane are measured using a quantity called the angular separation

$$\Delta R = (\Delta \eta^2 + \Delta \phi^2)^{1/2} \quad (3.1)$$

## 3.2.2 The ATLAS Detector Components

### 3.2.2.1 The Inner Detector

The Inner Detector (ID) [29], also called the tracker, is built to reconstruct trajectories of charged particles from which momenta can be computed. It is capable, at

high precision and high resolution, of momentum and primary vertex measurements. Moreover, it is also able to measure impact parameters and secondary vertices, and thus is capable of identifying heavy flavour jets.

Figure 3.4 illustrates the ID. The ID is 2.1 m in diameter and 6.2 m in length.

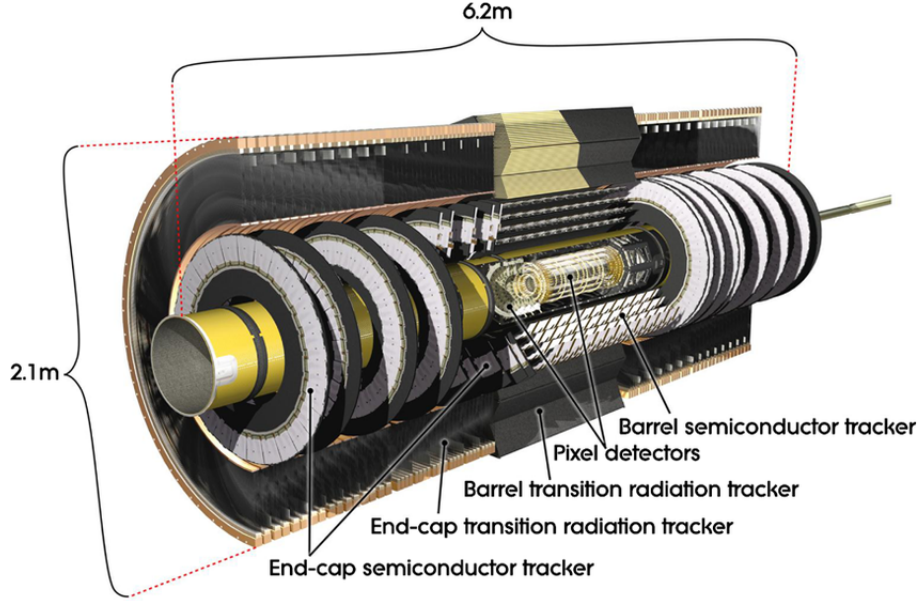


Figure 3.4: The ATLAS Inner Detector

The ID is surrounded by a 2T magnetic field parallel to the beam axis. This field deflects the paths of charged particles the curvatures of which are used for the measurements of their momenta and charges.

To achieve the desired performance, the ID is built up of semiconductor pixel and strip detectors in the inner part and straw-tube tracking detectors in the outer part. The pixel and the strip detectors are silicon detectors.

The ID is divided into three main components. Thus, the Pixel Detector and the semiconductor tracker (SCT) are to work in combination with the transition radiation tracker (TRT).

The Pixel Detector and the SCT work with each other to provide precision tracking near the interaction point. They cover the region  $|\eta| < 2.5$ . In terms of arrangement:

- In the barrel region, they lie on concentric cylinders around the beam axis.
- In the end-cap regions, they lie on disks perpendicular to the beam axis.

**The Pixel Detector** The Pixel Detector surrounds the beam pipe. Made up of silicon pixel detectors, it is able to cope with very high track density that is typically expected. It is constructed in the form of segmented layers of identical sensors in the  $R - \phi$  plane and along the  $z$ -axis, where the sensors are of size  $50 \times 400 \mu\text{m}^2$ . Typically, a track is expected to cross three such layers. The achieved accuracies in



the barrel are approximately  $10\text{ }\mu\text{m}$  in the  $R - \phi$  plane and  $115\text{ }\mu\text{m}$  in the  $z$  direction. The Pixel Detector has approximately 80.4 millions readout channels.

In May 2014, an additional pixel layer was installed between the pixels and the beam spot, at a distance of 3.3 cm from the beam pipe. It is called the insertable B-layer (the IBL [35]) and provides an additional 8 millions pixels. The results are improvements in track reconstruction, vertex measurement, and b-jet identification.

**SCT** A track is typically expected to cross eight strip layers of the SCT. In the barrel region, the  $R - \phi$  coordinates are measured by small-angle stereo strips that lie along the beam direction, and which are distributed one set per layer. In the end-cap regions there are two sets of strips, one running radially and one at a small angle. The accuracies achieved in the barrel are  $17\text{ }\mu\text{m}$  in the  $R - \phi$  plane and  $580\text{ }\mu\text{m}$  in the  $z$  direction, while those in the disks are  $17\text{ }\mu\text{m}$  in the  $R - \phi$  plane and  $580\text{ }\mu\text{m}$  in the  $R$  direction. The SCT has approximately 6.3 millions readout channels in total.

The Pixel Detector and the SCT function at small radii.

**TRT** The TRT measures only  $R - \phi$  coordinates and covers the region  $|\eta| < 2.0$ . It consists of straw tubes, 4mm in diameter, that typically register 36 hits per track. Each straw tube achieves an accuracy of  $130\text{ }\mu\text{m}$ . In terms of arrangement:

- In the barrel region, the straw tubes are manufactured at length 144 cm and lie parallel to the beam axis.
- In the end-cap regions, they are manufactured at length 37 cm and lie radially, in wheels.

The ID system supplements the calorimeters and the muon detector, which will be discussed below.

### 3.2.2.2 The Calorimeters

Calorimeters are built to measure energies of particles, using the facts that particles interact with the detector materials along their paths and cause radiation in the process. The ATLAS calorimeters [29, 36] consist of two systems, the Electromagnetic Calorimeter and the Hadronic Calorimeter, designed to measure the energies of electrons/photons and hadrons respectively.

An outline of the calorimeter system is shown in Figure 3.5. The required resolutions are

- The Electromagnetic Calorimeter:  $\sigma_E/E = 10\%/\sqrt{E} \oplus 0.7\%$
- The Hadronic Calorimeter:  $\sigma_E/E = 50\%/\sqrt{E} \oplus 3\%$  (barrel and end-cap regions),  $\sigma_E/E = 100\%/\sqrt{E} \oplus 10\%$  (forward region).

711 where each resolution is a quadratic combination of two separation terms, one,  
 712 called the stochastic term, that takes into account the statistical nature of the shower  
 713 shape, and one constant term that includes the effects of detector instabilities and  
 714 mis-calibration. The effect of the stochastic term decreases with growing energy.

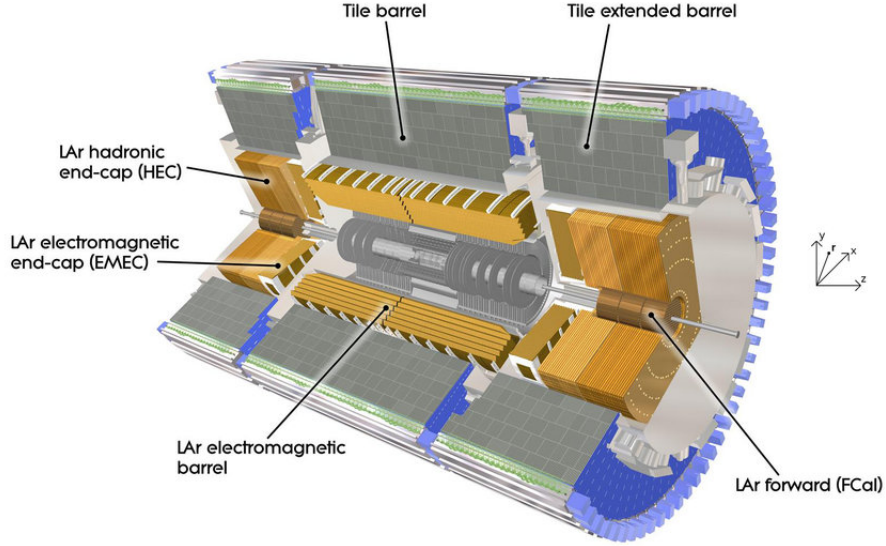


Figure 3.5: The ATLAS Calorimeter System

[32]

715 **The Electromagnetic Calorimeter** The Electromagnetic Calorimeter provides  
 716 electron and photon identification and kinematic measurements. These particles  
 717 lose their energies mainly through bremsstrahlung, pair production, and ionization,  
 718 where the first two dominate for high-energy particles, leading to the development  
 719 of shower shapes in the calorimeter.

720 By design, the Electromagnetic Calorimeter is a lead-LAr (Liquid Argon) detec-  
 721 tor. The lead, in the form of lead plates, functions as an absorber, and the liquid  
 722 argon is used in the active layers.

723 There are:

- 724 • The barrel part, covering  $|\eta| < 1.475$ , which is  $> 22$  radiation lengths in  
 725 thickness.
- 726 • Two end-cap components, covering  $1.375 < |\eta| < 3.2$ , where each is  $> 24$   
 727 radiation lengths in thickness.

728 The barrel is made up of two identical half-barrels, with a gap of 4 mm in between  
 729 at  $z = 0$ . On the other hand, each end-cap is made up of an outer wheel that covers  
 730 the region  $1.375 < |\eta| < 2.5$  and an inner wheel that covers the remaining region.

731 There is a presampler detector, which is an active LAr layer of 1.1 cm in thickness  
 732 in the barrel and 0.5 cm in thickness in each end-cap, covering the region  $|\eta| < 1.8$ .  
 733 It is used to correct the energy lost by electrons and photons in the materials they  
 734 traverse before they reach the calorimeter, such as those in the inner detector.



The Electromagnetic Calorimeter is complemented by the Hadronic Calorimeter, discussed in more detail below. Together, they contain electromagnetic and hadronic showers and limit penetration into the muon system.

**The Hadronic Calorimeter** The Hadronic Calorimeter surrounds the Electromagnetic Calorimeter. It is built to measure energy of hadronic particles, which also show up in the form of showers in the calorimeter.

In terms of thickness, the Hadronic Calorimeter is approximately 10 interaction lengths in the barrel region as well as in the end-cap regions. It is divided into three parts:

- Tile calorimeter: A sampling calorimeter, where steel is used as the absorber and scintillating tiles as the active material. It is placed directly outside the EM calorimeter envelope. It has a barrel that covers the region  $|\eta| < 1.0$  and two extended barrels which cover the region  $0.8 < |\eta| < 1.7$ , each made up of three layers.
- LAr hadronic end-cap calorimeter: The Hadronic End-cap Calorimeter covers the pseudorapidity range  $1.4 < |\eta| < 3.2$ . It is also a sampling calorimeter, where copper in the form of plates functions as the absorber and LAr gaps as the active medium. It has two independent wheels per end-cap. The wheels are put directly behind the end-cap electromagnetic calorimeters. Those closest to the interaction points use 25 mm parallel copper plates, and the rest uses 50 mm copper plates. The copper plates extend a radius from approximately 0.4 m to approximately 2 m, and in between are gaps of LAr materials.
- LAr forward calorimeter: The Forward Calorimeter extends the coverage up to  $|\eta| = 5$ , and is approximately 10 interaction lengths in depth. It has three modules in each end-cap, with one (copper) optimized for electromagnetic measurements and the remaining two (tungsten) hadronic measurements. Each module is a metal matrix of longitudinal channels, where the channels are filled with electrode structure which are in turns made up of concentric rods and tubes parallel to the beam axis, with LAr between them.

### 3.2.2.3 The Muon Spectrometer

Muons, being more massive than electrons (approximately 200 times), are subject to reduced bremsstrahlung as compared to electrons, and are able to pass through the ATLAS calorimeters with minimal interactions. The Muon Spectrometer [29] provides muon identification as well as muon momentum and charge measurement. It is capable of identifying muon candidates with  $p_T$  from 3 GeV and has a design resolution of 10% for muons with  $p_T = 1$  TeV.

The Muon Spectrometer surrounds the hadronic calorimeter and defines the overall dimensions of the ATLAS detector (Figure 3.6). It is made up of three layers of precision tracking chambers plus trigger chambers.

Deflection of the muon tracks is effected by the built-in superconducting magnets, which is a system of three large air-core toroids. In detail,

- The barrel toroid provides deflection over the range  $|\eta| < 1.4$
- The end-cap magnets at both ends of the barrel toroid, over the range  $1.6 < |\eta| < 2.7$
- A combination of barrel and end-cap magnets, over the range  $1.4 < |\eta| < 1.6$  (also called the transition region)

Muon tracks are measured in the tracking chambers. They are the Monitored Drift Tubes over most of the  $|\eta|$ -range, and Cathode Strip Chambers at large  $|\eta|$ -range. The chambers are arranged in the following manner:

- Around the beam axis, in the form of three cylindrical layers
- In the transition ( $1.4 < |\eta| < 1.6$ ) and end-cap regions, in three planes perpendicular to the beam

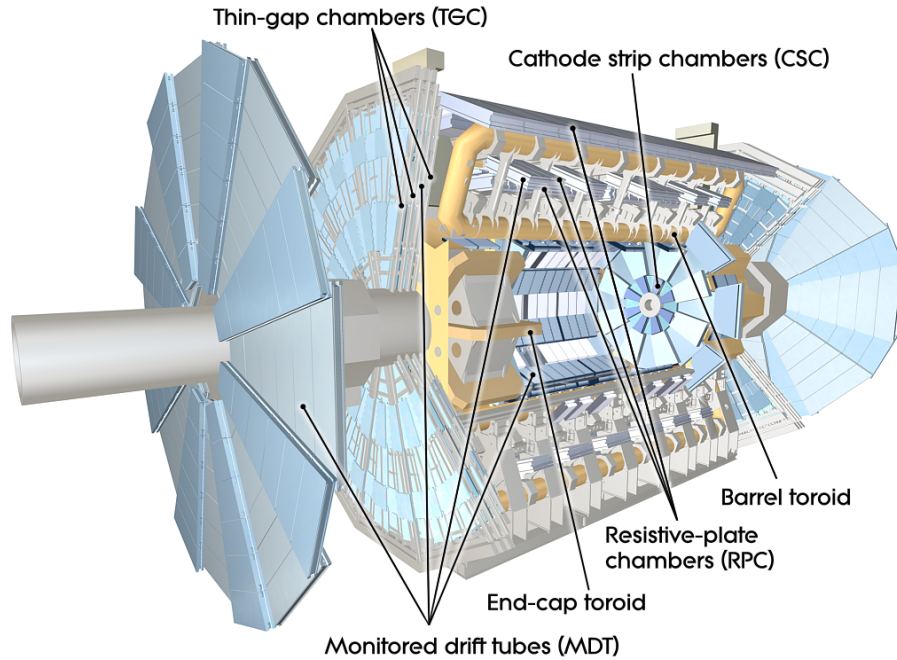


Figure 3.6: The ATLAS Muon Spectrometer

The trigger system works in the range  $|\eta| < 2.4$ . The trigger chambers, which are Resistive Plate Chambers in the barrel and Thin Gap Chambers in the end-cap regions, provide the following functionalities:

- Bunch-crossing identification
- Well-defined transverse momentum thresholds
- Measurements muon coordinate in the direction orthogonal to that determined by the precision-tracking chambers.

### 3.2.3 The ATLAS Trigger System

Due to the high luminosity of the LHC, the ATLAS detector, with limited storage capacity and technology, is only able to record potentially interesting physics events. This is achieved in Run-2 with a trigger system made up of two levels, the hardware level L1 and the High Level Trigger (HLT) software trigger, which together helps reducing the event rate from approximately 30 MHz to approximately 1 kHz [37].

L1 helps reducing the rate to about 100 kHz, taking  $2.5 \mu\text{s}$  for each event. It identifies high transverse-momentum muons, electrons, photons, jets, and taus that decay into hadrons. It also searches for events with large missing and total transverse energy. L1 is implemented using custom-made electronics, and uses low-resolution information from the calorimeters and the muon spectrometer. An event passing L1 is defined one or more regions of interests — for examples the  $\eta$  and  $\phi$  coordinates where something potentially useful has been seen — before being passed to the HLT.

On the other hand, the HLT is a software-based trigger. It helps to reduce the event rate to about 1 kHz, using information either in the regions of interests defined by L1 or the whole event. At the HLT each event takes on average about 200ms.